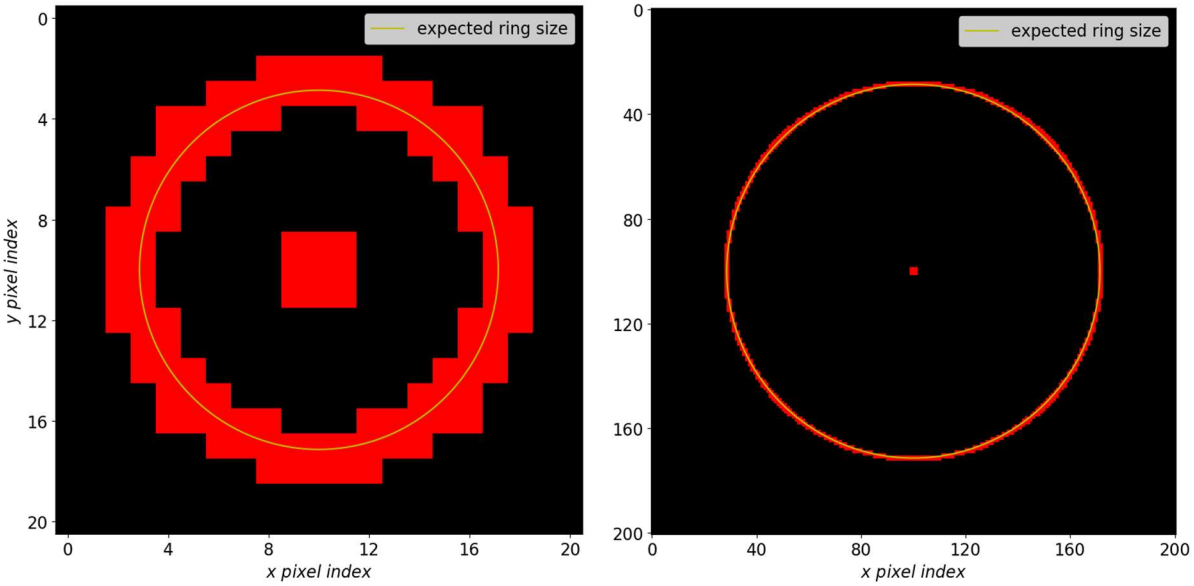

Figure.1 – Reproducing the test case.

(LEFT): Reproduced test case of the Einstein ring from centred, single pixel source; lensed by equations for a planar, transparent, smooth mass distribution. The source image size is (21×21) pixels and lensing is completed with core radius $r_c = 0.7$, and ellipticity $\varepsilon = 0$. The domain of reduced coordinates d is kept to $(-1,\ 1)$, giving $d = 1$. The full ring is produced as expected, at the pre-calculated radius (for $\varepsilon = 0: r = \sqrt{1 - r_c^2}$) and a plot of the predicted ring is overlaid.

(RIGHT): Same system scaled to a larger source image to ensure that the results correctly scale up. It uses (201×201) pixels with 1 pixel centre source and all same parameters. The code still clearly reproduces correct, expected behaviour, the ring is still full, is of approximately equal thickness throughout, and lies at the expected radius. Image was produced to show the basic functionality of the code written to complete lensing.

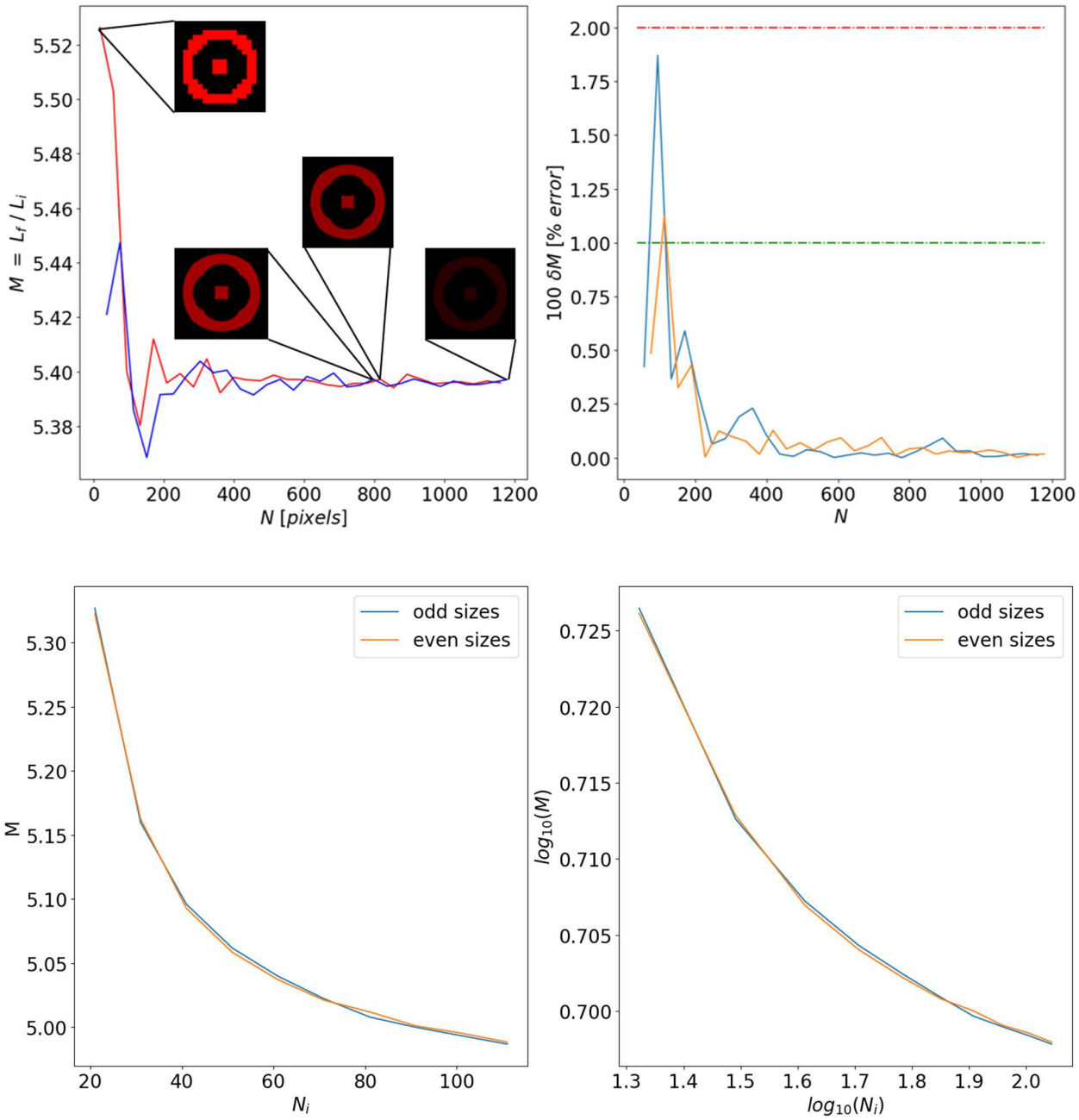

Figure 2 – Convergence study of centre pixel magnification M, with resolution.
Size of image was increased to observe convergence with resolution. For consistency, starting image must remain of the same proportions and with same total starting Luminosity L_i defined to be the sum of all RGB values for all pixels. To account for this, beginning with an image of size $(N_i \times N_i)$ with a single pixel in the centre (4 central pixels, value $\frac{1}{4}$ for even N_i) with $L = 1$, each pixel was equally divided (allowing for a better resolution). The result after each divide was lensed ($r_c = 0.7, \varepsilon = 0, d = 1$) and final L_f was found. Magnification was defined as the fractional change in L.

Top row:
(LEFT) Convergence of odd (red) and even (blue) image sizes (from splits on initially odd N_i). (RIGHT) Percentage error for each found magnification measurement, as a fractional change between neighbouring points. Shows random errors with 1% (green) and 2% (red).

Bottom: Investigated systematic error in the measurement.

(LEFT) The end convergence value dependence on N_i. (RIGHT) same variation on logarithmic scaling. Expected variation $M \sim \frac{a}{N_i^p} + b$. Future studies may consider completing the process in reverse order, beginning with maximal resolution and averaging to lower pixel values. The advantage of that would a known, constant, underlying structure. Positive outcome of this study is known minimal resolution $N \gtrsim 200$ for convergence, despite varying M with N_i.

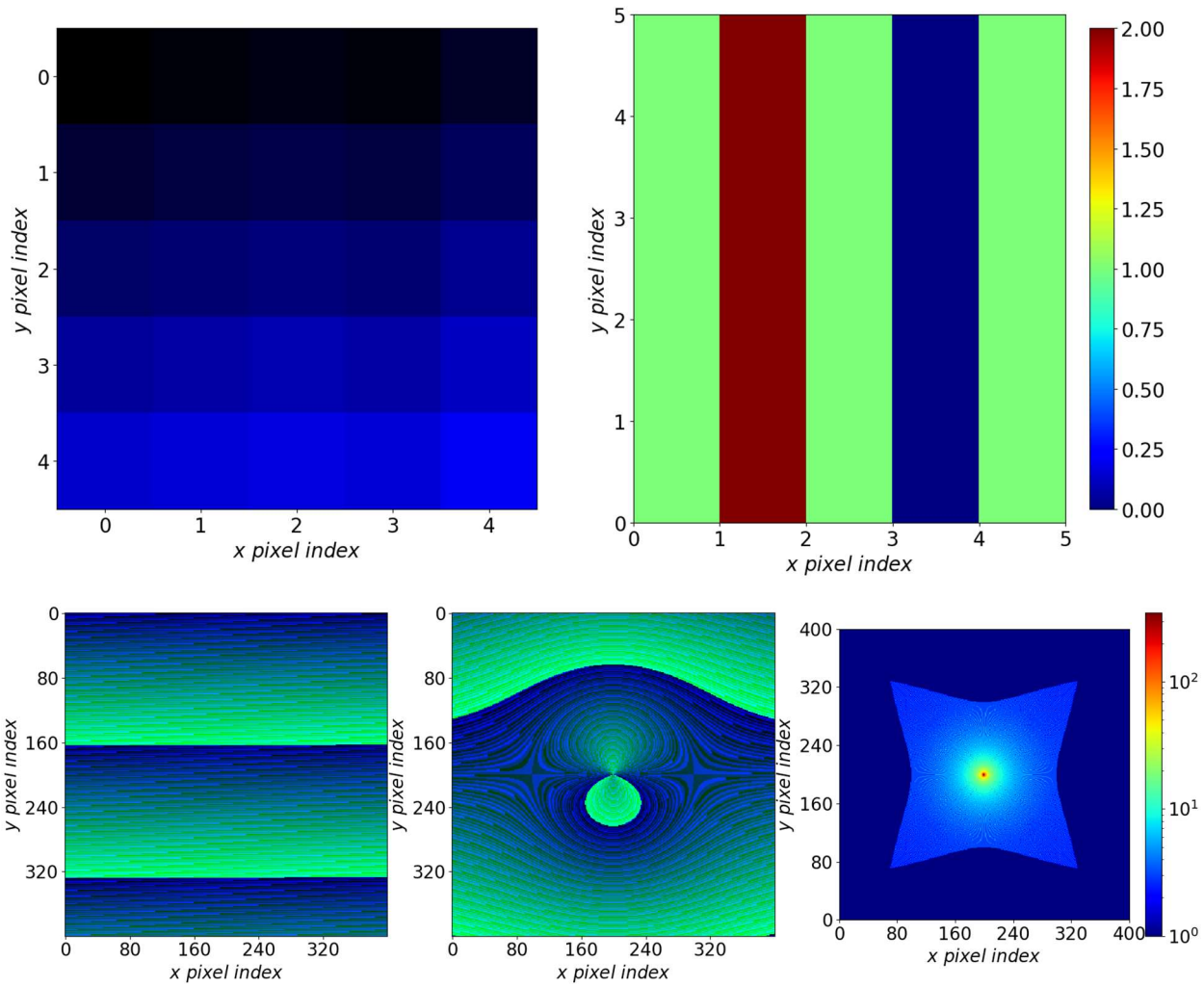

Figure 3 – Magnification M map of the source plane. Completed to represent lensing strength for all positions in the source plane.

Top row:

(LEFT) Test image (5×5 pixels) marked with RGB values unique to each position. (RIGHT) Column 2 data has replaced data in column 4, and the unique RGB values have been searched for to give a plot of the number of occurrences. Shows the expected result of 1 occurrence for unedited data, 0 occurrences of RGBs from column 4 and twice occurrence from column 2.

Bottom row: Source image (400×400 pixels) with same RGB marking, lensed, with parameters $r_c = 0$, $\varepsilon = 0$, $d = 2$. Gives relative magnification for each pixel of the image.

(LEFT) Original source image, with RGB tagging. (MIDDLE) lensed image. (RIGHT) the resulting magnification map plotted on a logarithmic colour scale $\log_{10}(1 + M)$. The pixels from image edges have been magnified by 0 ($\log_{10}(1 + M) = 0$), these project outside of the image plane. The lighter blue star patters occur as more distance exists to corners of image plane than to sides (by $\times \sqrt{2}$). Near centre, the expected circularly symmetric pattern is observed. Lighter blue pattern shows small scale artefacts of unknown origin. Extensive searching for their origin was attempted with a null result.

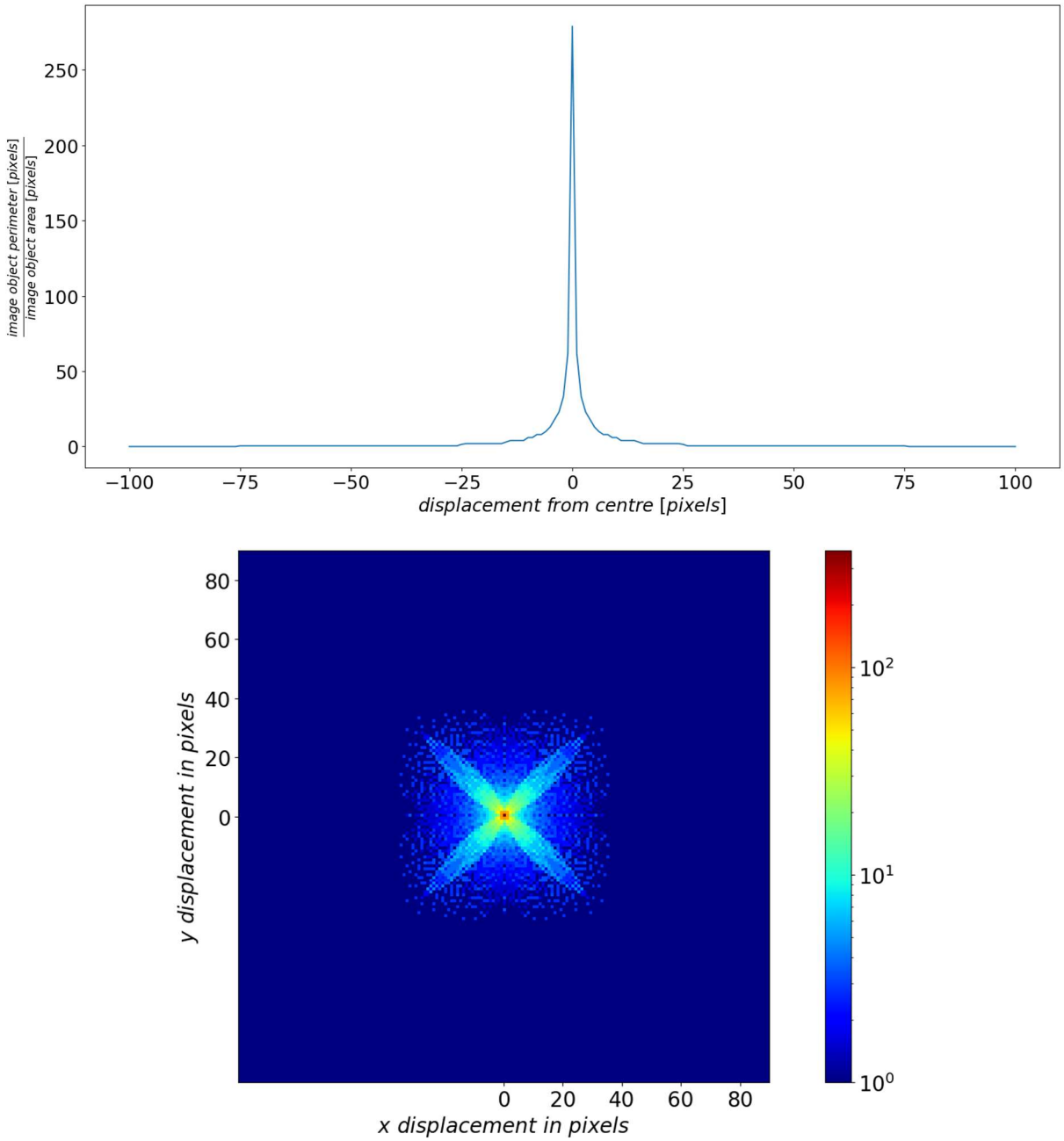

Figure 4 – 1D and 2D maps of shape distortions.

Shape distortions have been parametrised by the ratio of perimeter to area of the created image. The area was measured as the number of non-zero valued pixels and the perimeter was measured using the perimeter finder from an image analyser library called skimage. The ratio for the original, single pixel source was set to 1.

(Top) Graph of the ratio for different displacements of the single pixel source from the centre of the source image, along the x axis. Maximum shape distortions occur at the centre when the single pixel is lensed to form the full Einstein ring. As the displacement form the centre increases, the shape distortions rapidly decrease.

(Bottom) Logarithmically scaled map of shape distortions for different displacement of the source pixel in the 2D source plane. Colours indicate the value of the perimeter to area ratio ($+1$ for the logarithmic scaling). It is in general agreement with the 1D plot of displacement along the x axis only (above). The artefacts along the diagonals were studied, but a general conclusion explaining their

origin cannot be drawn. Future expansions should include more rigorous testing of the used methods to find the limitation of this model that causes these results. Results are concluded to be incorrect.

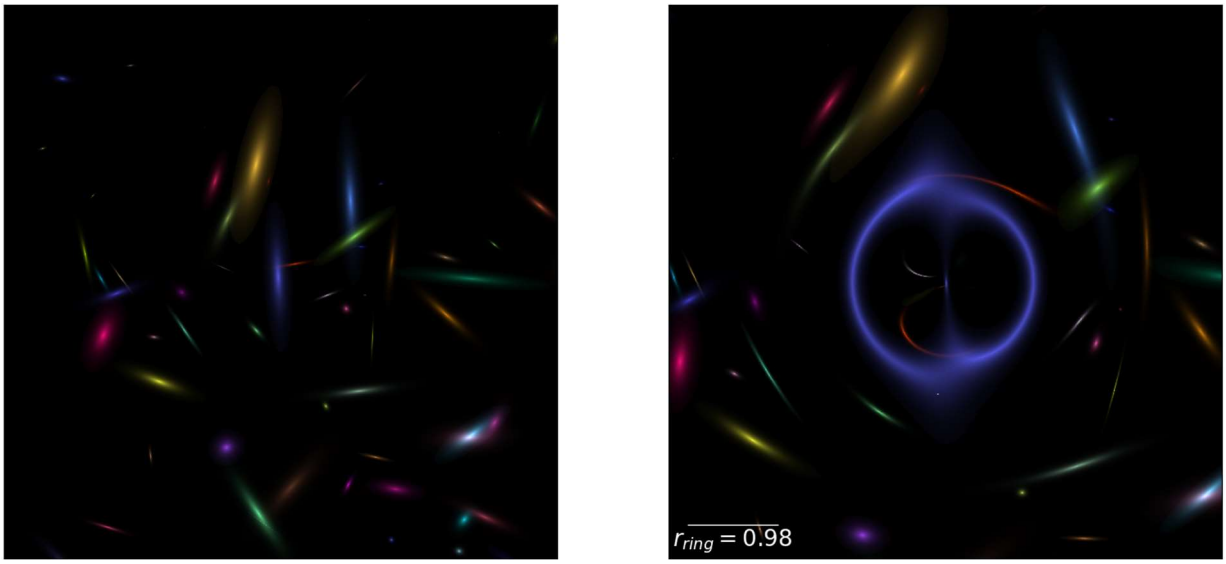

Figure.5 – Generating and lensing a galaxy cluster.
(LEFT): Generated cluster of 70 galaxies on a (2048×2048) pixel image. The flux profile of all galaxies follows: $f(r) = f_0 e^{-\frac{r}{a}}$. Galaxies have randomly generated: positions, angles to horizontal, RGB colours (f_0), decay constants(a) in range $(0,\ 0.32)$ pixels, minor axis in range $(1,\ 80)$ pixels and major axis ensured to be larger than minor axis in range $(minor, 4 * minor)$. For each galaxy, the r parameter in the flux profile has been transformed using the standard 2D rotation matrix R. The image has been seeded for reproducibility.
(RIGHT): Lensed image of generated galaxies (lensing parameters: $r_c = 0.2,\ \varepsilon = 0$) and with domain of reduced coordinates $d = 3$. The image clearly demonstrates the effect of far galaxies being stretched and pushed to further radii as expected from Figure.3. It is also clear that the galaxy (blue) passing through the centre of the lens produces a nearly ideal Einstein ring with expected radius $(r \sim \frac{1}{3} \cdot d)$. Galaxies near the centre can be viewed twice in the lensed image, as expected for objects positioned within the caustic of the lens.

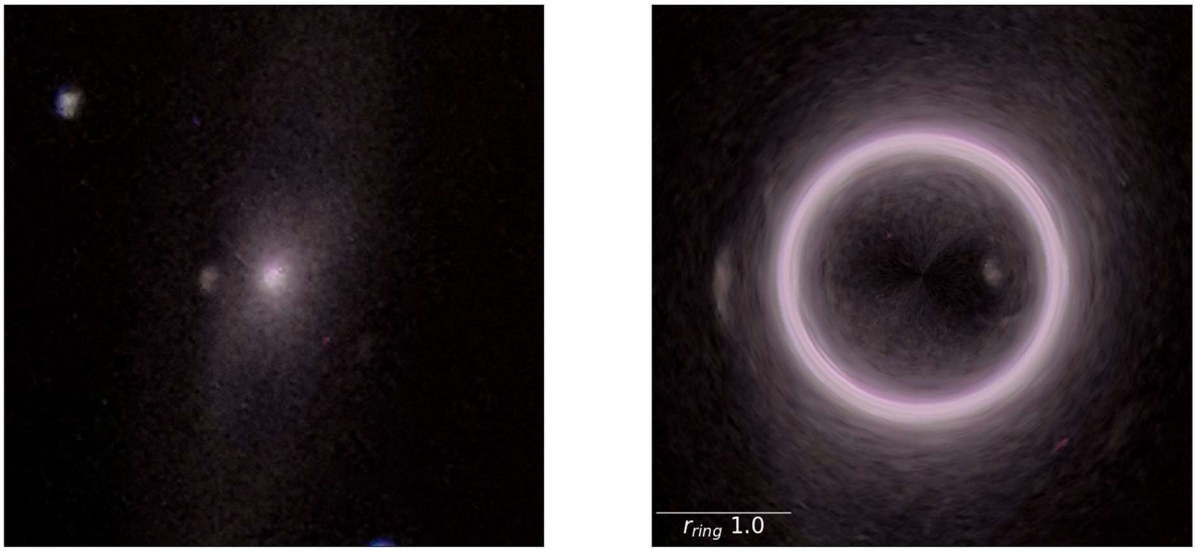

Figure.6 –jpg image lensed using a black hole lens ($r_c = 0$)
(LEFT): Original jpg image of Messier 65 (credit: Maciej Tomasz Jarema, using Bresser Messier telescope). The jpg was cut to a square size of (1121×1121) pixels.
(RIGHT): Lensed jpg image with black hole lens $r_c = 0$, and with $\varepsilon = 0,\ d = 2$. As expected, an Einstein ring is formed, of the expected size (here $r = \sqrt{1 - 0^2} = 1$). It is clear that the star (brown, left of centre) is seen twice in the lensed image, as would be expected for objects within the lens caustic. The same is true for the red feature (lower right of centre).
This lensing of a jpg has also been made into an animation, where it is moved into the lensing plane. The (RIGHT) figure here is the same as the last animation frame.

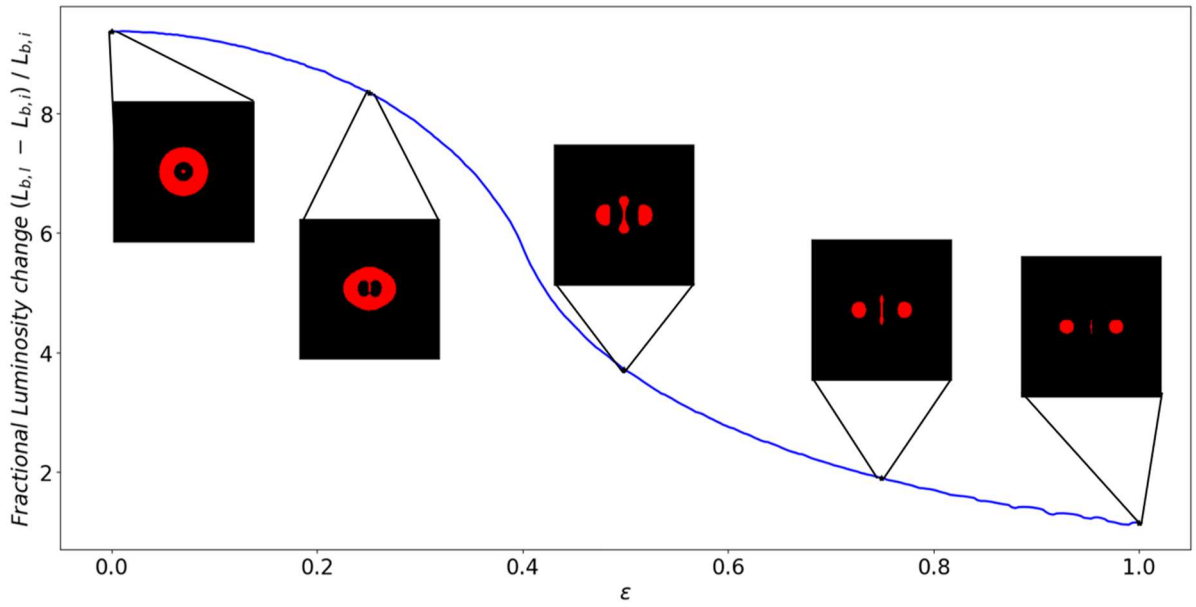

Figure.7 – Parameter study, effect of lensing with varying ε on total luminosity.
An image (600×600 pixels) of a circular source (radius 30 pixels, RGB set to 1, 0, 0) has been lensed with varying ellipticities ε (with $r_c = 0.2$, $d = 4$) and the integrated luminosity L_b for each has been found. The fractional difference of these has then been found between the lensed image $L_{b,l}$ and the original $L_{b,i}$. That fractional difference has been plotted for ellipticities in range $(0, 1)$. Inset plots demonstrate examples of seen images at ellipticities: $0.00, 0.25, 0.50, 0.75$ and 1.00.
Initially, the source forms as Einstein ring, as expected. As ellipticity is increased, luminosity L_f decreases as the Einstein ring is stretched horizontally and its core vertically expands. Further increases in ellipticity result in lensed images tending to a standard result of two images separated by a thin stretched line. This line is the image of the central object passing right through the highly elliptical lens, causing it to only magnify in one direction (vertically). The luminosity fraction tends to a constant $\frac{\Delta L}{L_i} \sim 1.157$.

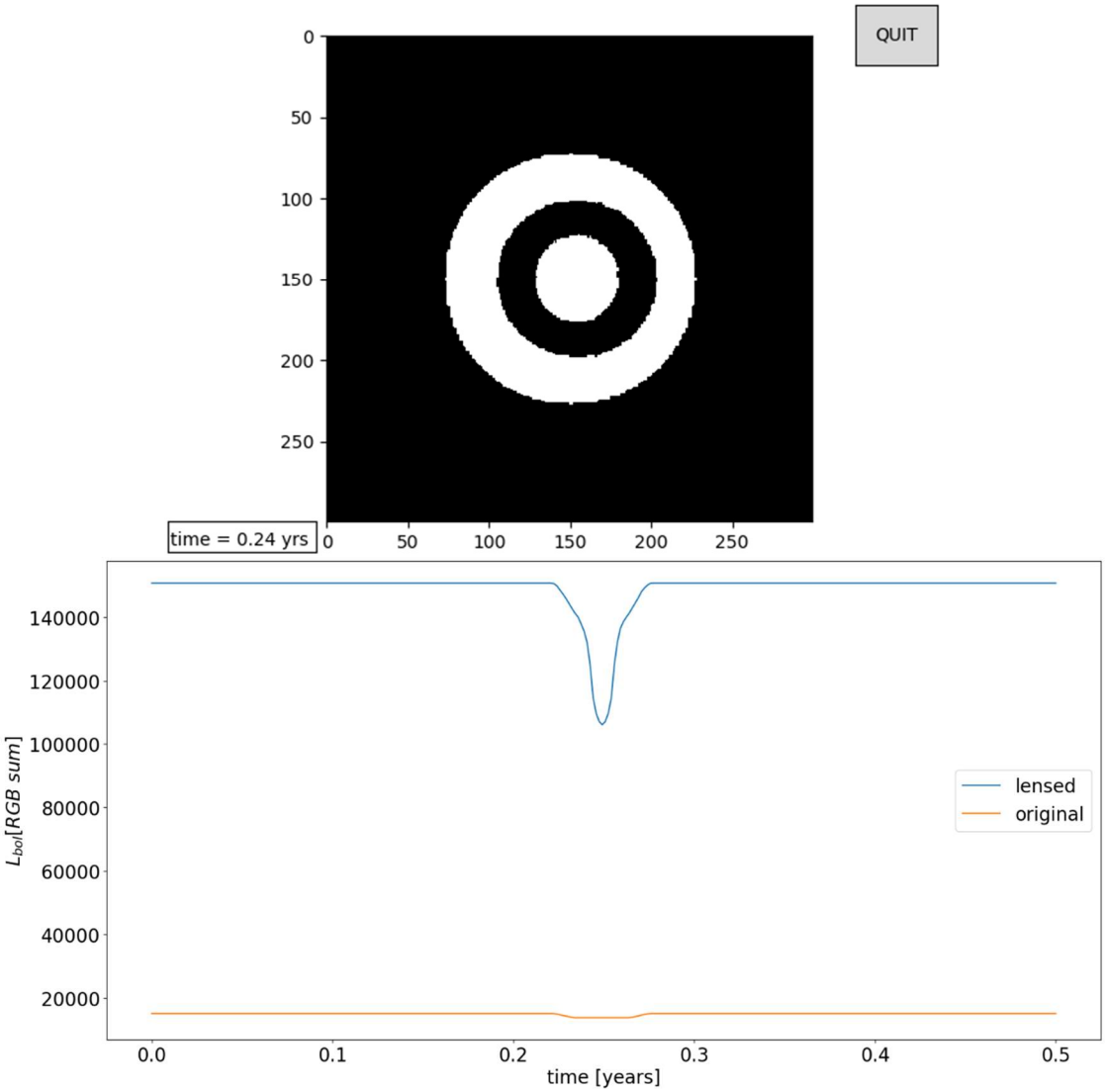

Figure 8 – Simulated 2 body lensed transit.

2 body motion has been implemented in 2 dimensions and projected to side view (view along y axis). The simulated data (for Earth Sun system, duration$= 0.5yr$) for centres of the 2 bodies has been used to generate pixelated (800×800) images of the two bodies with given radii (specified by user), by a function written to complete pixelated drawings (by me, for this project).

(Top): A snapshot from the simulation, with Sun size of 40 pixels, Earth size of 12 pixels (not to scale, models a less dense planet than earth).

(Bottom) The Luminosity (as previously defined) has been measured at every time step of the simulation for both the original image and the lensed view. The light curves have been plotted. From these, ratios of Planet radius to star radius have been found. The true ratio is defined such that: $\left(\frac{R_p}{R_s}\right)^2 = \left(\frac{12}{40}\right)^2 = 0.09$. The found ratio from transit data was $\left(\frac{R_p}{R_s}\right)^2 \sim 0.088$. The ratio found from lensed data was: $\left(\frac{R_p}{R_s}\right)^2 \sim 0.296$. This sparked reason for an investigation into the effect of lensing on the measured ratio, this could not conclude in the limited time of the project. For more detail look at the '(star + planet) ratio vs Rp plot' file.

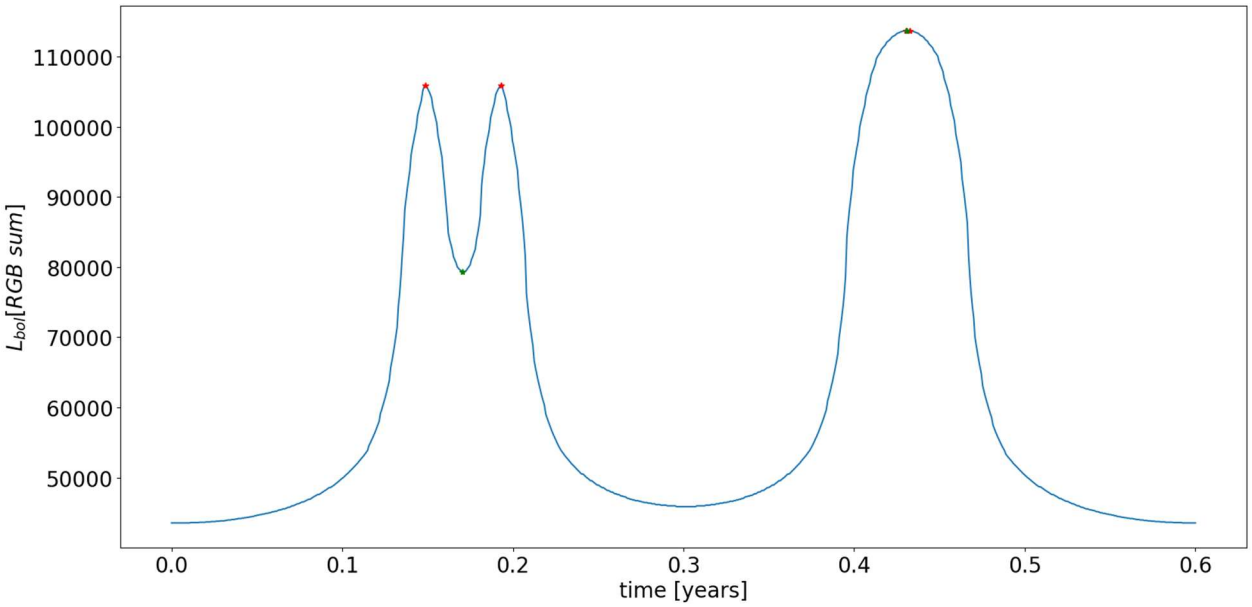

Figure 10 – Lensed binary orbiting a common centre of mass. Extracting ratio of body radii.

Using the same technique as for the Sun-Earth-like transits with different parameters (equal masses $2 \times 10^{30}\ kg$ and larger separation of $1AU$), light curves have been constructed for lensed ($r_c = 0.15,\ \varepsilon = 0, d = 6$) two bodies orbiting a common centre of mass. One object is assumed to be much dimmer than the other, such that its luminosity can be approximated as zero (RGB $= 0\ , 0, 0$). Via lensing, the two bodies get magnified, brighter bodies' luminosity increases and the area the dim object obscures does so. This competing effect causes the first, double peak. The Centre of Mass of the two is aligned with the centre of the lensing plane, therefore both peaks (Bright positive – eclipse and Dark negative - transit) align. At $\sim 0.43yr$ the eclipse occurs when the planet moves behind the star and does not cause any effect on its luminosity. Comparing the ecclipse maximum (red stars) to the transit minimum (lower green star), the ratio of radii can be approximated. This is done by $\left(\frac{R_p}{R_s}\right)^2 = \frac{L_{max} - L_{min}}{L_{max}}$. Giving $\left(\frac{R_p}{R_s}\right) \sim 0.3025$, the true ratio for used sizes was $\left(\frac{R_p}{R_s}\right) \sim 0.3$. A systematic overestimate is known to exist over many attempts from rigorous testing. The effects of the Centre of Mass not being aligned to the lens plane have also been investigated, but the analysis becomes much more difficult to handle. It is also worth noting that, it is a toy model, such a system is not expected to be observed. This is because the binary body must be resolved, with a strong lensing source in between, and the three planes cannot displace with respect to one another throughout a whole orbit of the binary. Thus, it would have to exist outside of the Milky Way, and hence the binary is not expected to be resolvable.